# Fiber-Optic Observation of Volcanic Tremor through Floating Ice Sheet Resonance

**Journal Article**

**Author(s):**
Fichtner, Andreas; Klaasen, Sara; Thrastarson, Sölvi; Çubuk-Sabuncu, Yeşim; Paitz, Patrick; Jónsdóttir, Kristín

**Publication date:**
2022-07-06

**Permanent link:**
https://doi.org/10.3929/ethz-b-000567658



**Originally published in:**
The Seismic Record 2(3), https://doi.org/10.1785/0320220010

**Funding acknowledgement:**
821115 - Real-time Earthquake Risk Reduction for Europe (EC)

The Seismic Record
A journal of the Seismological Society of America

# Fiber-Optic Observation of Volcanic Tremor through Floating Ice Sheet Resonance

Andreas Fichtner*[1], Sara Klaasen[1], Solvi Thrastarson[1], Yeşim Çubuk-Sabuncu[2], Patrick Paitz[1], and Kristín Jónsdóttir[2]

## Abstract

Entirely covered by the Vatnajökull ice cap, Grímsvötn is among Iceland's largest and most hazardous volcanoes. Here we demonstrate that fiber-optic sensing technology deployed on a natural floating ice resonator can detect volcanic tremor at the level of few nano-strain/s, thereby enabling a new mode of subglacial volcano monitoring under harsh conditions. A 12.5 km long fiber-optic cable deployed on Grímsvötn in May 2021 revealed a high level of local earthquake activity, superimposed onto nearly monochromatic oscillations of the caldera. High data quality combined with dense spatial sampling identify these oscillations as flexural gravity wave resonance of the ice sheet that floats atop a subglacial lake. Although being affected by the ambient wavefield, the time–frequency characteristics of observed caldera resonance require the presence of an additional persistent driving force with temporal variations over several days, that is most plausibly explained in terms of low-frequency volcanic tremor. In addition to demonstrating the logistical feasibility of installing a large, high-quality fiber-optic sensing network in a subarctic environment, our experiment shows that ice sheet resonance may act as a natural amplifier of otherwise undetectable (volcanic) signals. This suggests that similar resonators might be used in a targeted fashion to improve monitoring of ice-covered volcanic systems.

**Cite this article as** Fichtner, A., S. Klaasen, S. Thrastarson, Y. Çubuk-Sabuncu, P. Paitz, and K. Jónsdóttir (2022). Fiber-Optic Observation of Volcanic Tremor through Floating Ice Sheet Resonance, *The Seismic Record*. **2**(**3**), 148–155, doi: 10.1785/0320220010.

**Supplemental Material**

## Introduction

Grímsvötn is among Iceland's largest and, on a decadal time scale, most active volcanoes. It is located within a dense cluster of major volcanoes beneath the Vatnajökull ice cap where the Iceland hotspot is centered (Wolfe *et al.*, 1997). Grímsvötn ranks among the most productive volcanic systems on Earth, being responsible for the 1783 Laki eruption, the largest ever witnessed by mankind, which affected climate on a global scale (Thordarson and Self, 2003). With a caldera of ~10 km in diameter, major eruptions occurred on average every 10 yr during the past century (Global Volcanism Program, 2012). The volcanic system is marked by the complex interaction of geothermal heating and ice melting, which leads to the formation of a subglacial lake. Occasional outburst floods cause inundations of the coastal plains and destruction of infrastructure (Gudmundsson *et al.*, 1997). Grímsvötn's caldera eruptions are explosive, as the interaction of basaltic magma, gases, and meltwater produces ash plumes of tens of kilometers height, which affect human lives, agriculture, livestock, and aviation.

The last major eruption started on 21 May 2011 and lasted for 8 days. The ash cloud, peaking at 20 km altitude, led to the cancellation of 900 flights and the closure of Iceland's main airport, Keflavik (Wunderman, 2011). In December 2021,

1. Department of Earth Sciences, ETH Zurich, Zurich, Switzerland, https://orcid.org/0000-0003-3090-963X (AF); https://orcid.org/0000-0003-0931-6776 (SK); https://orcid.org/0000-0003-4094-7891 (ST); https://orcid.org/0000-0003-0589-929X (PP); 2. Icelandic Meteorological Office, Reykjavik, Iceland, https://orcid.org/0000-0002-9572-3468 (YÇ-S); https://orcid.org/0000-0001-7464-224X (KJ)

*Corresponding author: andreas.fichtner@erdw.ethz.ch

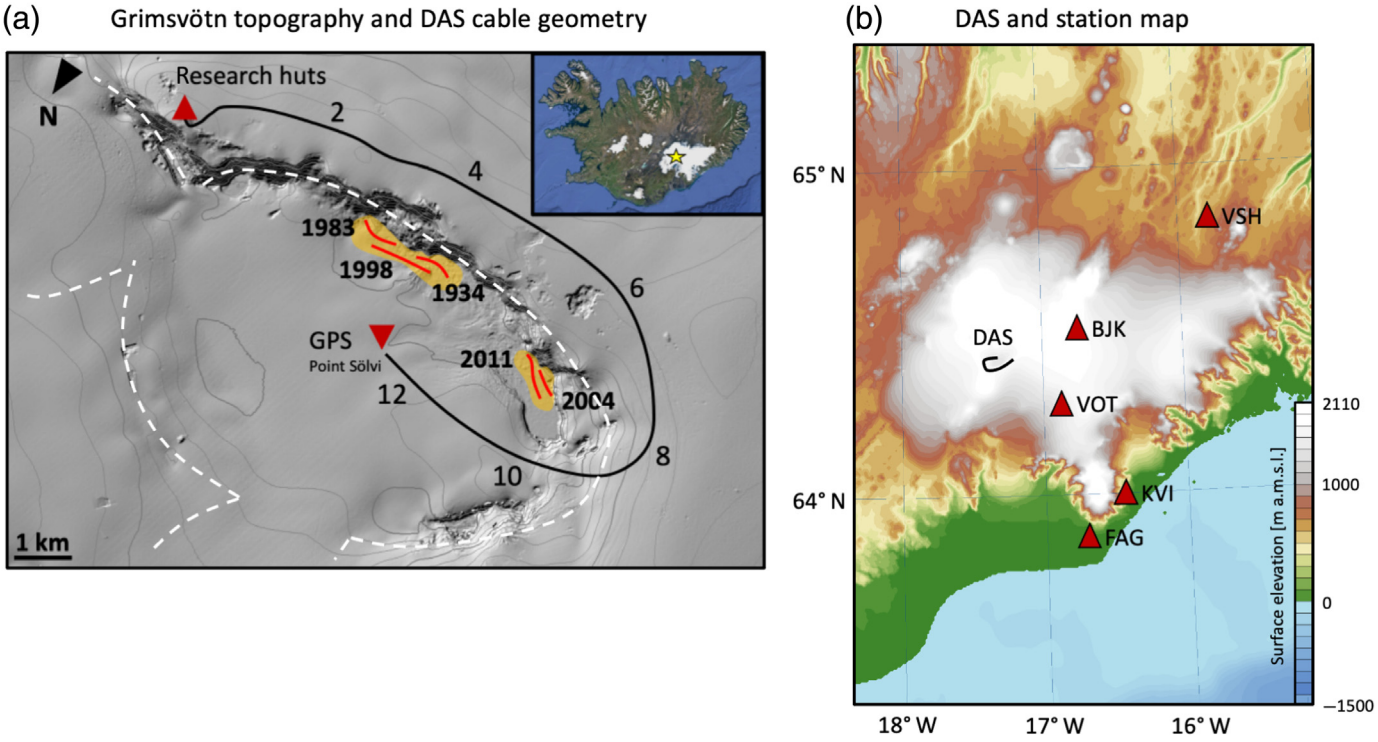


**Figure 1.** Setup of the experiment. (a) Layout of the cable along the crater rim and inside the caldera of Grímsvötn, with distance along the cable in kilometer. The locations of the research huts and the end point of the cable near the Global Positioning System (GPS) station are shown as red triangles. Locations of the previous fissure eruptions are shown in orange and red, and the outline of the caldera is approximated by the with dashed curve. (b) Location of the Distributed Acoustic Sensing (DAS) experiment (black curve) in southern Iceland and locations of broadband seismic stations used for comparison (red triangles). Topographic information is taken from ArcticDEM (Porter *et al.*, 2018). The inset shows a map of Iceland, with the location of Grimsvötn indicated by a yellow star.

Grímsvötn's showed increased activity, including elevated seismic activity, ice sheet subsidence by nearly 80 m, and drainage of more than 0.8 $km^3$ of water from the subglacial lake (Global Volcanism Program, 2021).

The ongoing activity of Grímsvötn and the size of its historic eruptions call for detailed geophysical monitoring, which is, however, complicated by the remoteness of the site and its harsh environmental conditions. Within this context, emerging Distributed Acoustic Sensing (DAS) technologies offer new opportunities for densely spaced deformation measurements in a broad frequency band from millihertz to kilohertz (Hartog, 2017; Lindsey *et al.*, 2020; Paitz *et al.*, 2021; Lindsey and Martin, 2021). In particular, the relative ease of deploying a fibre-optic cable on a glacier yields a measurement density that would be difficult to achieve with conventional seismic instruments (Walter *et al.*, 2020; Klaasen *et al.*, 2021).

In spring 2021, we trenched 12.5 km of a Solifos BRUfield fiber-optic cable around and within the caldera of Grímsvötn using a custom-made sled, towed by a Snowcat (Klaasen *et al.*, 2022). In a research hut, located at Grímsfjall, the highest point of the caldera rim, we connected a single-mode fiber to a Silixa iDAS v2 interrogator. It collected strain rate measurements with 8 m channel spacing, 10 m gauge length, and 200 Hz sampling frequency for 3 weeks, starting on 6 May 2021. A summary of the experimental setup is shown in Figure 1. Although the thickness of the ice cap in the area is roughly constant around 300 m, the lake level varies over time scales of several years. Prior to flooding events as in December 2021, it may reach 100–150 m (Bethier *et al.*, 2006).

Despite its geologic complexity, we will show that many aspects of Grímsvötn's low-frequency seismic response can be understood in terms of simple effective physical systems.

## DAS Observations of Caldera Resonance

Figure 2 shows a typical record section that focuses on the last 4.5 km of the cable, largely located inside the caldera. Deformation with a dominant frequency above 10 Hz, induced by a local earthquake and reaching peak strain rates above 100 nanostrain/s, is clearly visible in Figure 2a, which shows a 40 s long record section starting at UTC01:00:30 on 7 May 2021.

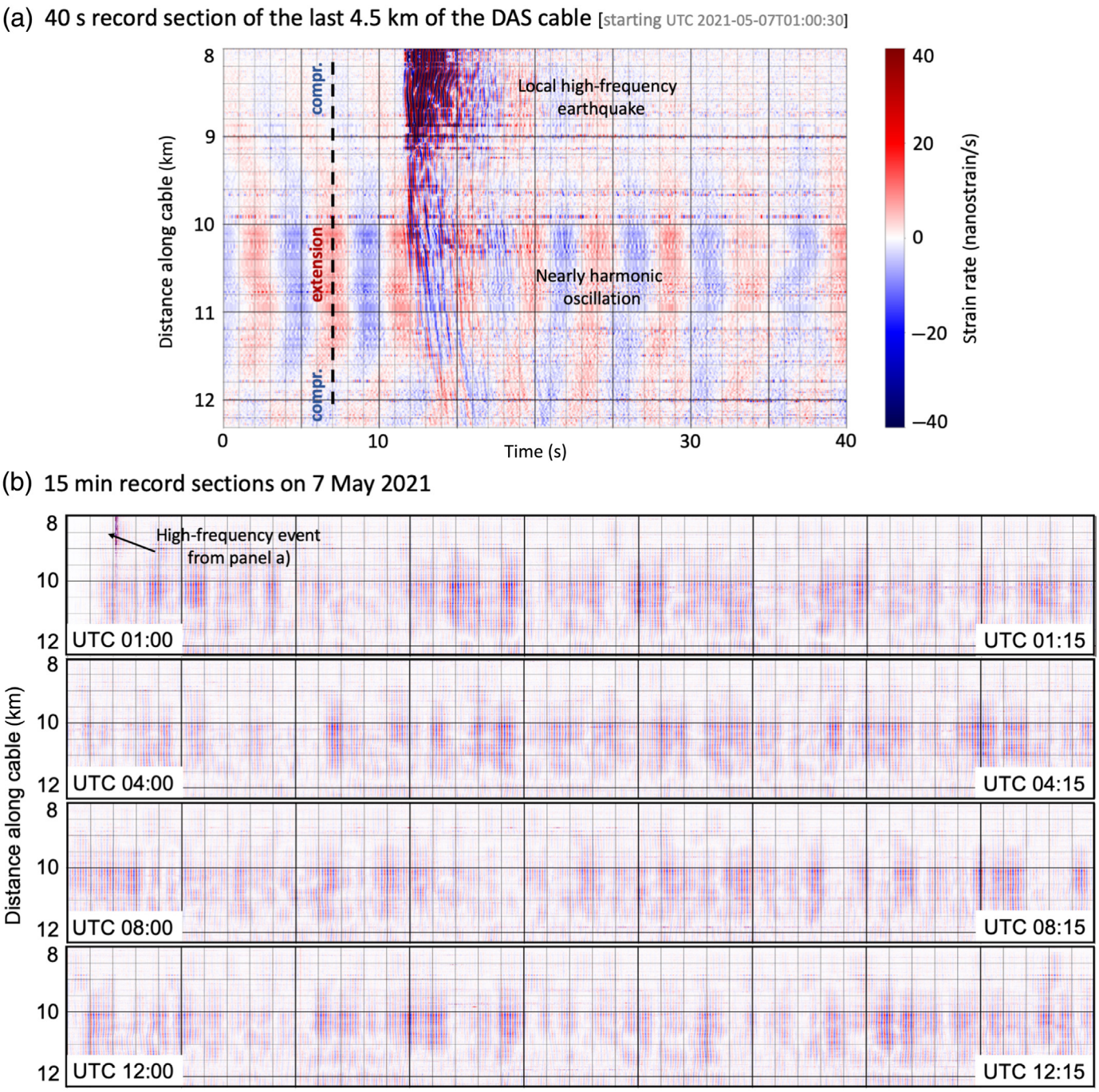


During the 3 weeks of the experiment, nearly 2000 similar local events could be detected (Thrastarson *et al.*, 2021). The earthquake signal is superimposed onto a nearly harmonic oscillation at lower frequency and maximum strain rates on the order of 10 nanostrain/s. As shown in Figure 2b, these oscillations persist during the morning hours of 7 May 2021, with slight variations on a one-minute time scale but overall constant peak amplitudes around 10 nanostrain/s.

**Figure 2.** DAS data collected along the last 4.5 km of cable inside the caldera (see Fig. 1) on 7 May 2021. (a) Record section of 40 s length starting at UTC 01:00:30. Deformation produced by a high-frequency local earthquake is superimposed on a nearly harmonic lower amplitude signal. (b) Selection of 15 min long record sections in the morning hours of 7 May 2021. The low-amplitude oscillations are continuously observable.

The densely sampled DAS data reveal that the low-frequency oscillations are not a localized phenomenon but affect the floating part of the ice sheet as a whole. As indicated, for instance, by the dashed vertical line in Figure 2a, the parts of the caldera between ~9.0 and ~11.5 km along the cable periodically extend, while adjacent parts compress, and vice versa. This suggests that we observe flexural gravity waves, i.e., oscillatory bending of the ice sheet coupled to gravity waves within the water layer, but also to the underlying solid Earth. Though being subject to different boundary conditions, these flexural gravity waves are similar to those in Antarctic ice shelves (Bromirski *et al.*, 2017; Lipovsky, 2018; Olinger *et al.*, 2022). With the limited coverage of the caldera, the complete mode shape can unfortunately not be estimated. It therefore remains unclear if we observe the fundamental mode or an overtone.

Spectral analyses of the DAS channels within the caldera, shown in Figure 3, quantify the bandwidth of the oscillations at half peak amplitude to $\Delta f \sim 0.02$ Hz around the dominant frequency $f_0 = \sim 0.22$ Hz. The width of the observed amplitude spectrum can largely be explained by that of a 1D damped harmonic oscillator,

$$|g(\omega)| = \left| \frac{A}{\omega_0^2 - \omega^2 + i\omega\omega_0 Q^{-1}} \right|, \quad (1)$$

in which $A$ denotes amplitude in strain/s$^2$, $\omega$ circular frequency, and $\omega_0 = 2\pi f_0$. The quality factor $Q$ controls the width of the peak and has a value of around 20. This suggests that the system as a whole, despite being 3D and geometrically complex, effectively behaves as a forced resonator that dissipates around $2\pi Q^{-1} \approx 31\%$ of its total energy per oscillation cycle. Figure 3a also confirms that the spectral amplitudes of the ice sheet oscillations are approximately constant in the morning hours of 7 May 2021.

These spectral properties are in contrast to the characteristics of the ocean wave-generated secondary ambient field (Peterson, 1993; Gualtieri *et al.*, 2013; Nakata *et al.*, 2019), shown for the coastal station KVI in Figure 3b, in which this contribution to the seismic wavefield is expected to be the largest. Compared to the ice sheet oscillations, ambient vibrations have a similar central frequency of ~0.28 Hz but with significantly larger bandwidth of $\Delta f \sim 0.07$ Hz and spectral amplitude variations of nearly 300% within only 12 hr. As shown in Figure S1, available in the supplemental material to this article, the spectral characteristics at station KVI are very similar to those at other stations in southern Iceland.

Figure 3c extends the spectral analysis of the DAS channels and station KVI to the whole duration of the experiment. The time-dependent spectra display visible correlations, suggesting that ambient vibrations are a significant driver of the ice sheet oscillations. However, there are several time periods when strong ice sheet oscillations could be observed, despite low ambient vibration amplitudes. These include, as seen before, the morning hours of 7 May 2021, but also others, extending from few hours to several days.

Though station KVI is only one among many in southern Iceland, it is still remarkably representative, as illustrated in Figures S1 and S2. The spectral properties of ambient vibrations recorded at broadband seismometers in southern Iceland are nearly identical. This leads to the important preliminary conclusions that the ambient field in the region is spectrally largely homogeneous, and that the anomalous oscillations in the Grímsvötn caldera require some residual driving forces.

## Estimation of Residual Driving Forces

Despite the complexity of the volcanic system, the nature of the data permits plausible simplifications to estimate the effective residual forces. At frequencies below ~0.3 Hz and seismic phase velocities in the range of several kilometers per second for volcanic rocks (Lowrie and Fichtner, 2020), the wavelengths of the ambient and residual deformations that drive ice sheet oscillation are on the order of 10 km. Consequently, the observations are largely insensitive to spatial variations of the forces at scales below the dimension of the Grímsvötn caldera. This allows us to represent them as space-independent quantities, as illustrated schematically in Figure 4a. Furthermore, the low deformation amplitude on the order of 10 nanostrain/s implies that the system is effectively linear. Hence, denoting by $F_k(\omega)$ the total effective force in time interval $k$, we have

$$F_k(\omega) = F\omega[u_k^{\mathrm{obs}}(\omega) + r_k(\omega)], \quad (2)$$

in which $u_k(\omega)$ is the observed ambient velocity spectrum, and $r_k(\omega)$ the yet unknown residual forcing. The proportionality factor $F$, with unit s/m, states that the effective force $F_k$ that drives the system should be linearly related to ground acceleration $\omega[u_k^{\mathrm{obs}}(\omega) + r_k(\omega)]$. Owing to the previously noted spatial homogeneity of the ambient field, we may use any vertical-component seismometer spectrum in southern Iceland for $u_k^{\mathrm{obs}}(\omega)$. In the following, we use the spectrum of station BJK (Fig. 1b), which is the closest to the Grímsvötn caldera.

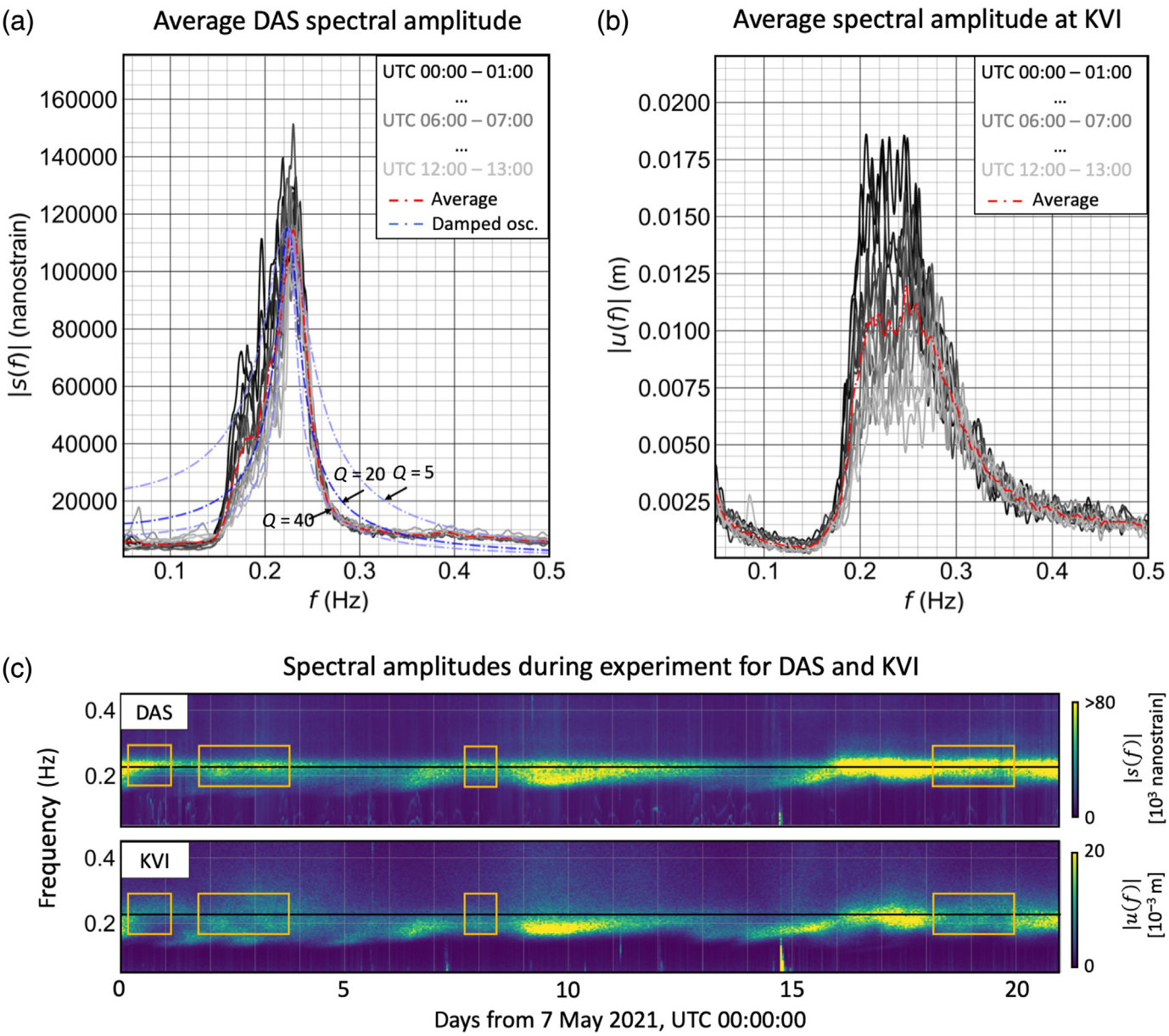


**Figure 3.** Spectral analysis of DAS channels and the coastal broadband seismic station KVI, shown in Figure 1. (a) Average spectral amplitude as a function of frequency, $|s(f)|$, for the DAS channels inside the caldera for one hour time intervals between midnight (black) and noon (light gray) on 7 May 2021. Shown in red is the average over all one hour intervals. The blue curves are the amplitude spectra of 1D damped harmonic oscillators with different $Q$ values. (b) Spectral amplitude $|u(f)|$ of the vertical component velocity at the seismic station KVI during the same time intervals and with identical color coding as in panel (a). The red curve is again the average over all time intervals. (c) Time evolution of the spectral amplitudes of DAS channels inside the caldera and the vertical velocity at KVI. The orange boxes mark periods in which changes in spectral amplitude at KVI do not correlate with changes in spectral amplitude at the DAS channels. The color scale of the DAS spectra saturates at $10^3$ nanostrain to enhance visibility of lower amplitude features.

Taking the effective system response $g(\omega)$ from equation (1), we may model the oscillation spectrum as

$$s_k(\omega) = F_k(\omega)g(\omega). \tag{3}$$

For given $F$ and $Q$, the residual forcing can be found through the solution of a linear least-squares problem (Tarantola, 2005; Fichtner, 2021). Combining this with a grid search, yields values for $F$ and $Q$ that minimize the norm of

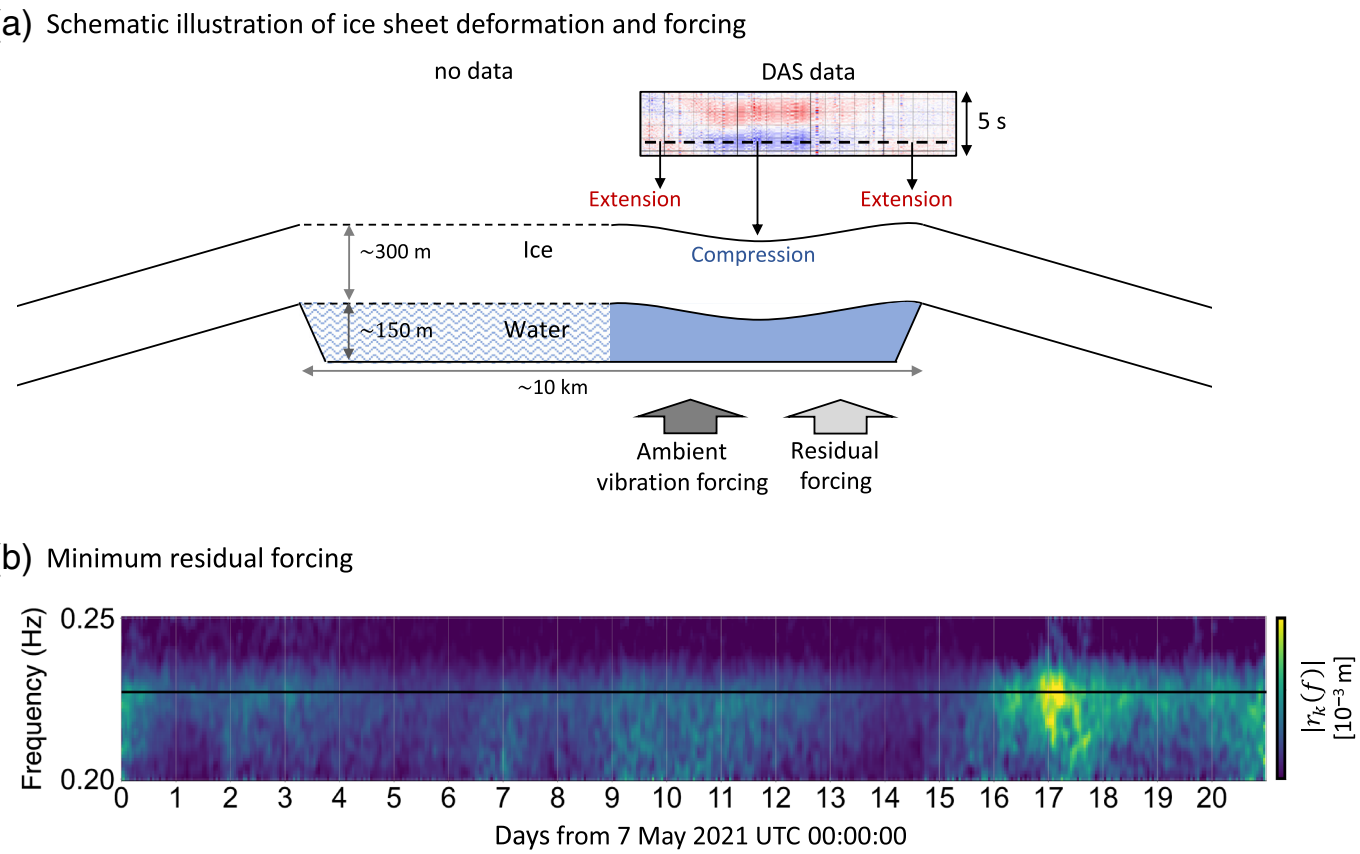


**Figure 4.** Residual forcing of ice sheet resonance. (a) Conceptual illustration of ice sheet resonance in the eastern part of the caldera in which DAS data are available. Flexural bending leads to observations of alternating extension and compression. The inset shows an exemplary 5 s section of data extracted from Figure 2a. The ambient vibration and residual forcings are shown schematically as gray arrows. (b) Minimum residual forcing $r_k(f)$ in hourly intervals needed to explain ice sheet oscillations to within the observational errors.

$r_k(\omega)$, thereby providing the minimum residual forcing as a function of frequency and time interval, displayed in Figure 4b. The minimum residual forcing produces a root mean square misfit between observed spectra $s_k^{\text{obs}}(\omega)$ and modeled spectra $s_k(\omega)$ of 1.65, for an observational error standard deviation of $20 \times 10^3$ nanostrain, estimated conservatively from hourly amplitude spectra of the DAS channels. Furthermore, the amplitudes of the minimum residual forcing are significantly above the noise level of the seismometer recordings and in fact comparable to the ambient seismic noise amplitudes. This indicates that our simplistic model explains the observations to within their errors, and that no additional model complexities are required. A more detailed, time- and frequency-dependent analysis of the remaining difference between $s_k^{\text{obs}}(\omega)$ and $s_k(\omega)$ can be found in Figure S3.

## Discussion and Conclusions

As shown in Figure 4b, the inferred minimum residual forces acted continuously during the experiment and at least within the frequency band covered by the caldera resonance peak. Temporal variations occurred over several days, with a pronounced activity peak around day 17 (24 May 2021).

Local seismicity is unlikely to be a major contributor to the observed resonance for two reasons. First, local event signals have frequencies significantly above 1 Hz and therefore cannot excite resonance at 0.22 Hz. Second, even around 0.22 Hz, the damping of the resonator attenuates transient signals to below the noise level within less than a minute. This is significantly shorter than the average interevent duration of ~15 min (Thrastarson *et al.*, 2021). A similar argument excludes glacial flow, amounting to ~5 cm/day as a source, because it acts in a far lower frequency band.

In the context of earlier observations of low-frequency continuous seismic signals at other volcanoes (Kawakatsu *et al.*, 2000; De Martino *et al.*, 2005; Wassermann, 2012), the residual forces can plausibly be explained in terms of volcanic tremor. In the absence of visible magmatism in May 2021, the tremor is likely to be caused by geothermal activity, which has clear surface expressions in the form of fumaroles and cauldrons near the eastern flank of the caldera rim.

It would clearly be desirable to model the ice shelf oscillation in greater detail. Although this would technically be possible using spectral-element wavefield simulations that permit complex geometries (Komatitsch and Vilotte, 1998; Afanasiev *et al.*, 2019), the required pieces of information are not available. This includes, the most importantly, detailed maps of ice thickness and lake depth, which can vary substantially over weeks, that is, more rapidly than any 2D geophysical survey could be repeated.

In the same context, it is important to note that more complex physical models with a larger number of free parameters than the 1D damped harmonic oscillator are not required by the available data. This is because the observations can already be explained to within the errors by a single residual forcing term. Therefore, Bayes' theorem would ensure that models with more parameters are automatically less plausible. As a consequence, the residual forcing must be understood as an effective force that encapsulates individual forcing mechanisms that our data cannot resolve.

Regardless of the interpretation, it is evident that the floating ice sheet acts as an amplifier of signals that may otherwise be overwhelmed by ambient and instrumental noise. This suggests that similar natural resonators might be used in a targeted fashion for the monitoring of subglacial volcanoes, including, for example, Katla and the Skaftár cauldrons. Yet, while amplifying certain information, the resonance within a narrow frequency band also eliminates other frequencies that may be needed to infer more detailed source properties (Chouet, 1996; Lipovsky and Dunham, 2015).

Finally, our experiment demonstrates the logistical feasibility of installing a large fiber-optic sensing network in a subarctic environment in which the deployment of a similar array of conventional seismic instruments would not be possible. Trenching the cable ~30 cm into the ice provides a data quality that permits the detection of deformation as small as few nanostrain/s at frequencies from ~0.1 to 20 Hz. This study thereby paves the way toward dense seismic monitoring of remote, glacier-covered volcanoes under harsh environmental conditions.

## Data and Resources

The Grímsvötn Distributed Acoustic Sensing (DAS) dataset has a volume of around 1 TB, making it too large for remote access and download. However, the dataset will be made available on hard drives upon request. A video showing some fieldwork impressions can be found at https://www.youtube.com/watch?v=J7cxVZvgyWQ&t=0s (last accessed June 2022).

## Declaration of Competing Interests

The authors acknowledge that there are no conflicts of interest recorded.

## Acknowledgments

The authors gratefully acknowledge phenomenal support from Silixa throughout all stages of this experiment. This work was partially funded by the Real-time Earthquake Risk Reduction for a Resilient Europe project (RISE) under the European Union's Horizon 2020 research and innovation programme (Grant Agreement Number 821115). Constructive comments by Brad Lipovsky and an anonymous reviewer helped us to improve the article.

## References

Afanasiev, M. V., C. Boehm, M. van Driel, L. Krischer, M. Rietmann, D. A. May, M. G. Knepley, and A. Fichtner (2019). Modular and flexible spectral-element wave form modelling in two and three dimensions, *Geophys. J. Int.* **216,** doi: 10.1093/gji/ggy469.

Bethier, E., H. Bjornsson, F. Palsson, K. L. Feigl, M. Llubes, and F. Remy (2006). The level of the Grimsvotn subglacial lake, Vatnajokull, Iceland, monitored with SPOT5 images, *Earth Planet. Sci. Lett.* **243,** 293–302.

Bromirski, P. D., Z. Chen, R. A. Stephen, P. Gerstoft, D. Arcas, A. Diez, R. C. Aster, D. A. Wiens, and A. Nyblade (2017). Tsunami and infragravity waves impacting Antarctic ice shelves, *J. Geophys. Res.* **122,** 5786–5801.

Chouet, B. A. (1996). Long-period volcano seismicity: Its source and use in eruption forecasting, *Nature* **380,** 309–315.

De Martino, S., M. Falanga, R. Scarpa, and C. Godano (2005). Very-long-period volcanic tremor at stromboli, Italy, *Bull. Seismol. Soc. Am.* **95,** no. 3, 1186–1192.

Fichtner, A. (2021). *Lecture Notes on Inverse Theory*, Cambridge Open Engage, doi: 10.33774/coe-2021-qpq2j.

Global Volcanism Program (2012). Grimsvotn (373010), in *Volcanoes of the World, v. 4.10.5 (27 Jan 2022)*, Venzke, E. (Editor), Smithsonian Institution, doi: 10.5479/si.GVP.VOTW4-2013.

Global Volcanism Program (2021). Report on grimsvotn (Iceland), in *Weekly Volcanic Activity Rept., 1 December–7 December 2021*, Sennert, S. K. (Editor), Smithsonian Institution and US Geological Survey, Washington, D.C.

Gualtieri, L., E. Stutzmann, Y. Capdeville, F. Ardhuin, M. Schimmel, A. Mangeney, and A. Morelli (2013). Modeling secondary microseismic noise by normal mode summation, *Geophys. J. Int.* **193,** 1732–1745.

Gudmundsson, M. T., F. Sigmundsson, and H. Bjornsson (1997). Ice-volcano interaction of the 1996 Gjalp subglacial eruption, Vatnajokull, Iceland, *Nature* **389,** 954–957.

Hartog, A. (2017). *An Introduction to Distributed Optical Fibre Sensors*, CRC Press, Boca Raton.

Kawakatsu, H., S. Kaneshima, H. Matsubayashi, T. Ohminato, Y. Sudo, T. Tsutsui, K. Uhirae, H. Yamasatof, H. Ito, and D. Legrand (2000). Aso94: Aso seismic observation with broadband instruments, *J. Volcanol. Geotherm. Res.* **101,** nos. 1/2, 129–154.

Klaasen, S., P. Paitz, N. Lindner, J. Dettmer, and A. Fichtner (2021). Distributed acoustic sensing in volcano-glacial environments—Mount Meager, British Columbia, *J. Geophys. Res.* **159,** doi: 10.1029/2021JB022358.

Klaasen, S., S. Thrastarson, A. Fichtner, Y. Cubuk-Sabuncu, and K. Jonsdottir (2022). Sensing Iceland's most active volcano with a "buried hair", *Eos Trans. AGU* **103,** doi: 10.1029/2022EO220007.

Komatitsch, D., and J. P. Vilotte (1998). The spectral element method: An effective tool to simulate the seismic response of 2D and 3D geological structures, *Bull. Seismol. Soc. Am.* **88,** 368–392.

Lindsey, N. J., and E. Martin (2021). Fiber-optic seismology, *Annu. Rev. Earth Plant. Sci.* **49,** 309–336.

Lindsey, N. J., H. Rademacher, and J. B. Ajo-Franklin (2020). On the broadband instrument response of fiber-optic DAS arrays, *J. Geophys. Res.* **125,** doi: 10.1029/2019JB018145.

Lipovsky, B. P. (2018). Ice shelf rift propagation and the mechanics of wave-induced fracture, *J. Geophys. Res.* **123**, 4014–4033.

Lipovsky, B. P., and E. M. Dunham (2015). Vibrational modes of hydraulic fractures: Inference of fracture geometry from resonant frequencies and attenuation, *J. Geophys. Res.* **120,** 1080–1107.

Lowrie, W., and A. Fichtner (2020). *Fundamentals of Geophysics*, Cambridge University Press, Cambridge, United Kingdom.

Nakata, N., L. Gualtieri, and A. Fichtner (2019). *Seismic Ambient Noise*, Cambridge University Press, Cambridge, United Kingdom.

Olinger, S. D., B. P. Lipovsky, M. A. Denolle, and B. W. Crowell (2022). Tracking the cracking: a holistic analysis of rapid ice shelf fracture using seismology, geodesy, and satellite imagery on the Pine Island glacier ice shelf, west Antarctica, *Earth Space Sci. Open Arch.* doi: 10.1002/essoar.10510107.

Paitz, P., P. Edme, D. Graff, F. Walter, J. Doetsch, A. Chalari, A. Chalari, C. Schmelzbach, and A. Fichtner (2021). Empirical investigations of the instrument response for distributed acoustic sensing (DAS) across 17 octaves, *Bull. Seismol. Soc. Am.* **111,** 1–10.

Peterson, J. (1993). Observations and modeling of seismic background noise, *U.S. Geol. Surv. Open-File Rept. 93-322*, 94 pp.

Porter, C., P. Morin, I. Howat, M.-J. Noh, B. Bates, K. Peterman, S. Keesey, M. Schlenk, J. Gardiner, K. Tomko, *et al.* (2018). *ArcticDEM*, Harvard Dataverse, doi: 10.7910/DVN/OHHUKH.

Tarantola, A. (2005). *Inverse Problem Theory and Methods for Model Parameter Estimation*, Second Ed., Society for Industrial and Applied Mathematics, Philadephia.

Thordarson, T., and S. Self (2003). Atmospheric and environmental effects of the 1783-1784 Laki eruption: A review and reassessment, *J. Geophys. Res.* **108,** doi: 10.1029/2001JD002042.

Thrastarson, S., R. Torfason, S. Klaasen, P. Paitz, Y. Çubuk-Sabuncu, K. Jonsdottir, and A. Fichtner (2021). Detecting seismic events with computer vision: Applications for fiber-optic sensing, *Earth Space Sci. Open Arch.* doi: 10.1002/essoar.10509693.1.

Walter, F., D. Graff, F. Lindner, P. Paitz, M. Kopfli, M. Chmiel, and A. Fichtner (2020). Distributed acoustic sensing of microseismic sources and wave propagation in glaciated terrain, *Nat. Comm.* **11,** doi: 10.1038/s41467-020-15824.

Wassermann, J. (2012). Volcano seismology, in *New Manual of Seismological Observatory Practice 2 (NMSOP-2)*, Deutsches GeoForschungsZentrum GFZ, 1–77.

Wolfe, C. J., I. T. Bjarnason, J. C. VanDecar, and S. C. Solomon (1997). Seismic structure of the Iceland mantle plume, *Nature* **385,** 245–247.

Wunderman, R. (2011). Global volcanism program, 2011. Report on Grimsvotn (Iceland), *Bull. Global Volcanol. Netw.* **36,** doi: 10.5479/si.GVP.BGVN201106-373010.

Manuscript received 7 March 2022
Published online 6 July 2022